Medbiotech Journal

MBTJ, 4(2): 51-56, 2020

Research Paper

Recovery of Nanoparticles Bioproducts through Adsorption Process; Nanotechnology in Biotechnology Process

Basudeb Mondal*, Pinak Mandal

Department of Molecular Modeling, HiTech Institute of Theoretical and Computational Chemistry, India

Received: 02 April 2020 Accepted: 13 May 2020 Published: 01 June 2020

Abstract

The adsorbents employed in this study for the recovery of BSA and HSA nanoparticles had one of four discrete designs e.g. microporous (pore size <0.2 ∝m), macroporous (pore size >0.8 ∝m), solid phase (non-porous) and pellicular (pore size <0.5 ∝m). Soluble protein was included in the study to represent cellular components of complex feedstocks and the separation of assemblies from components, whilst nanoparticulate protein, served as surrogate size and charge mimics of less easily sourced viral and plasmid gene therapy vectors. Candidate adsorbents were physically characterized to assess their suitability for fluidized bed operation and biochemically characterized exploiting batch binding experimentation and laser scanning confocal microscopy. The adsorptive capacity of nanoparticulate products was strongly influenced by the physical design of the adsorbents and microporous adsorbents appeared to be less suited for the recovery of nanoparticulate products. The generic application of such adsorbents for the recovery of nanoparticulate bioproducts is strongly discussed.

Keywords: Protein nanoparticle, Surrogate Mimics, Bioproduct Recovery, Adsorbent Morphology, Fluidized Bed Adsorption.

How to cite the article:

B. Mondal, P. Mandal, Recovery of Nanoparticles Bioproducts through Adsorption Process; Nanotechnology in Biotechnology Process, Medbiotech J. 2020; 4(2): 51-56, DOI: 10.22034/MBT.2020.109579.

1. Introduction

Current chromatographic technology has been developed primarily for macromolecular products (1-5nm) and is not well suited for the recovery of nanoparticulate products such as plasmid DNA, viruses, macromolecular assemblies as drug delivery vehicles and virus like particles as vaccine components. due to the large size range of these products (20-300nm) and their complex surface characteristics [1-4] . Therefore, nanoparticulate products tend to be recovered by combination of ultracentrifugation and ultrafiltration protocols which are commonly scale limited, whilst dirty feedstocks such as cell lysates from animal cell and microbial cultures limit the efficiency such processes [5-7] .

Fluidised bed adsorption technology is an alternative that can be employed for nanoparticulate purification providing practical advantages such as the potential for direct process integration as has been seen with protein products [4-6]. However, this technology is limited since currently available adsorbent solid phases have characteristically small pore and particle diameters which have been optimized for the purification of protein rather than nanoparticulate products. Small pore size (5-400nm) limits the diffusion of the nanoparticulates (20-300nm) into the adsorbent solid phase and thus only the external surface area is available [8-10] .

In addition, low molecular weight contaminants (proteins, DNA, endotoxins etc.) will enter the pores resulting in a process requirement for

* Corresponding author email: Basudeb.m@iitcc.org

excessive washing steps to purge the internal volume of the adsorbent solid phase. Adsorbent solid phases have been designed with large macropores (1-3;m in diameter) allowing for convective flow within the solid phase, which could enable rapid adsorption and desorption characteristics. Pellicular solid phases should show shorter processing times due to the limited diffusion distances, but the loss of bulk capacity must be considered and the solid adsorbent circumvents diffusional limitations and the washing steps required due to the surface limited binding [11-14] . Therefore, the design and assembly of adsorbent particles is a critical factor to be considered to enable the successful operation of the recovery of nanoparticles. A study is reported herein which has investigated the binding of protein nanoparticles (60-200nm), fabricated from bovine or human serum albumin, as a viral size/charge mimic, to a selection of adsorbent solid phases characterised by a unique range of particle geometries and surface topographies [15-18] .

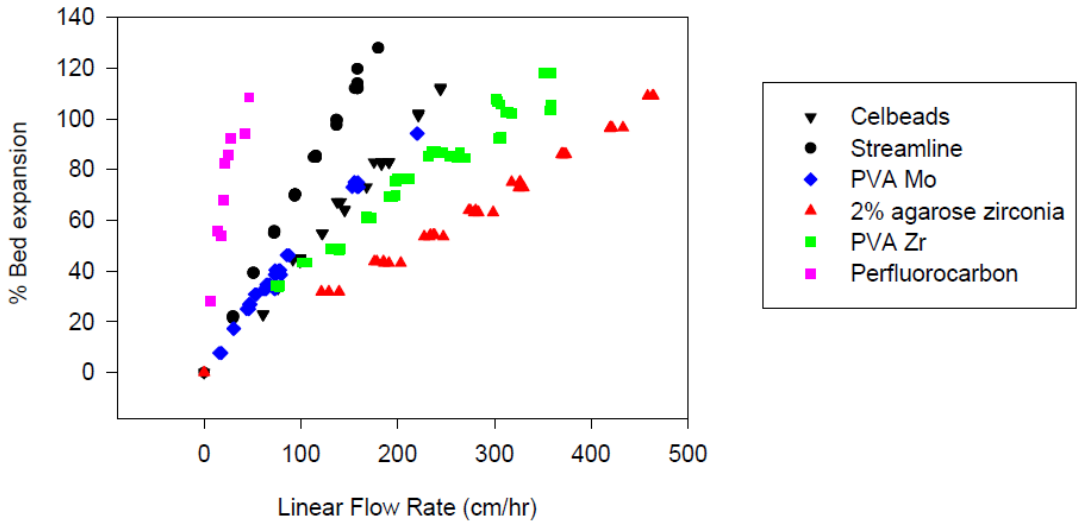

Figure 1. Bed expansion profiles of adsorbent solid phases. The bed expansion characteristics of the adsorbents were determined in fluidised beds operated with buffer A (10 mM Tris/HCl containing 0.2% (w/v) sodium azide at pH 7.5). The bed was allowed to settle for 15 minutes until stable and the bed height was measured against the flow rate entering the column.

2. Materials and Methods

All chemicals were purchased from Sigma or the Aldrich Chemical Company. Adsorbent solid phases used include commercial microporous adsorbents (Streamline), pellicular composites, solid particles (perfluorocarbon emulsions) and macroporous adsorbent particles (Cell beads, PVA composites). All adsorbents were derivatized with anion exchange chemistry (diethylaminoethyl, DEAE).

One of the major problems associated with such studies as this is the quantity of nanoparticulates required for experimentation with adsorbent capacities in excess of 10^{11} particles/ml adsorbent, hence sufficient quantities of nanoparticulates such as retrovirus and adenovirus are not available [8]. This problem has been circumvented by the use of synthetic nanoparticles fabricated from bovine and human serum albumin.

3. Results and discussion

3.1 Physical Characterization of Adsorbent Solid Phases

Adsorbent design implications incorporate both the suitability of the solid phase for nanoparticulate recovery and for fluidised bed operation, therefore the physical characteristics such as adsorbent size, density, pore size and small ion capacity of the adsorbent solid phases were investigated (Table 1). The commercial porous solid phase, Streamline, was used as a bench mark solid phase to which physical and biochemical characteristics were compared. All of the custom designed solid phases demonstrated good bed expansion characteristics in comparison to Streamline (Figure 1) except the solid perfluorocarbon adsorbent. This was due to the small size of the adsorbent; hence this solid phase was removed from the study due to poor bed expansion characteristics.

Table 1. Physical characteristics of adsorbent solid phases

Adsorbent	Size (m)	Density (g/ml)	Small Ion capacity (mol/ml)	Pore structure/pore size
Streamline	200	1.2	160	Microporous/ <200 nm
2% Agarose-zircona	240	1.67	89	Pellicular
Celbeads	394	1.38	41	Macroporous/ 5∝m
PVA Mo	423	1.39	27.8	Macroporous/ 1∝m
PVA Zr	514	1.37	54.4	Macroporous/ 1∝m
Perflurocarbon	10	2.1	8	Solid

Table 1 summarises the commercial and custom fabricated adsorbent solid phases that were included in the present study having different adsorbent configurations designated. The respective manufacturers supplied the data for pore size of the PVA and Celbead composites and the commercial adsorbents.

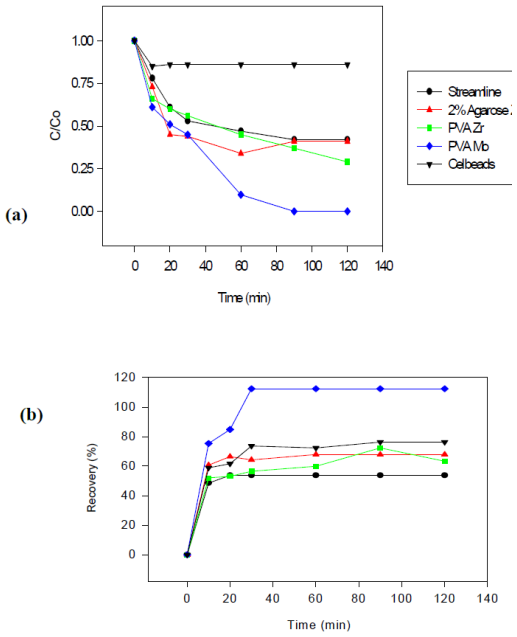

Figure 2. Batch binding and batch elution of BSA nanoparticles. 1004l of adsorbent was challenged with 1.5ml of BSA nanoparticles at a concentration of 2204g/ml in buffer A (10mM Tris-HCl, pH 7.5, 0.02% sodium azide, 0.01% Tween 20) for 2 hours. The decrease in concentration of the feedstock was measured over time (a). The adsorbent was subsequently washed five times with buffer A. The elution was then conducted in 1.5ml of 1.0M NaCl in buffer A and monitored over time. The recovery is expressed as a percentage of the estimated binding (b).

3.2 Biochemical Characterization of Adsorbent Solid Phases

The adsorption/desorption characteristics of the selected adsorbent solid phases were studied using batch binding experimentation. The binding and recovery profiles suggest that nanoparticulate recovery is affected by particle geometry (Figure 2). BSA nanoparticles adsorbed and desorbed rapidly on Cell beads, the adsorbent solid phase with the largest pore size (3 m) suggesting that the open pore structure of the adsorbent (60% pore volume) circumvented problems associated with diffusion limitations. However, the BSA nanoparticle capacity is low in comparison to the selected solid phases (Table 2.). 2% Agarose zirconia and Streamline both reached equilibrium within 30 minutes suggesting surface binding and limited penetration. In addition, the macroporous solid phases (PVA Zr and PVA Mo) demonstrated longer adsorption times (Figure 2) which is indicative of slow diffusion into the larger pores. Recovery of the BSA nanoparticles occurs within 30minutes for all the solid phases, however as shown in Table 2., with the exception of Celbeads and PVA Mo, the recoveries are generally poor (>70%). This could be due to slow diffusion from within the internal structure where there is nanoparticle penetration.

Table 2. Summary of BSA nanoparticle capacities and recoveries from preliminary batch binding experiments.

Adsorbent	Small Ion capacity (mol Cl/ml ads.)	BSA nanoparticle capacity (mg/ml ads.)	BSA nanoparticle capacity (particles/ml ads.)	Recovery %
Streamline	160	1.95	1.1×10^{12}	57.7
2%Agarosezircona	89	2.1	1.2×10^{12}	67.9
Celbeads	41	0.56	3.16×10^{11}	76.3
PVA Mo	27.8	0.9	5.08×10^{11}	~100
PVA Zr	54.4	1.67	9.4×10^{11}	63.3

Table 2 summarizes the adsorptive capacities and recoveries of BSAp calculated from batch adsorption and desorption studies. The capacity was determined by difference analysis of the initial load and the concentration after 120 minutes, whilst the recovery is the protein recovered as percentage of the protein adsorbed

Two different nanoparticulate mimics were used, both BSA nanoparticles (150nm in diameter) and HSA nanoparticles (70nm in diameter). The initial experiments were conducted using the larger BSA nanoparticles (Figures 2) with further studies investigating the adsorption/desorption of HSA nanoparticles (Figures 3) to the same solid phases. At this stage due to the poor capacity of Celbeads (Table 2) the adsorbent was removed from the study.

The adsorption/desorption characteristics of the selected adsorbent solid phases is different to that for BSA nanoparticles, which highlights the differences in structure. The macroporous adsorbents (PVA Mo and PVA Zr) show rapid adsorption profiles suggesting that the nanoparticles can pass freely into the pores, whilst the microporous adsorbents demonstrate a longer adsorption time. This could be attributable to the diffusion of the nanoparticles into the small pore structure. This is also confirmed from the slower desorption of the nanoparticles from Streamline and 2% agarose zirconia in comparison to PVA Zr and PVA Mo.

3.3 Laser Scanning Confocal Microscopy (LSCM)

The assumptions made about nanoparticle adsorption in relation to the adsorbent design based on adsorption profiles are validated using Laser Scanning Confocal Microscopy (LSCM). Figures 4 and 5 represent the adsorption of fluorescently labelled BSA nanoparticles to adsorbent solid phases characterized by different internal geometries. Figure 4 depicts limited surface binding of the BSA nanoparticles with the commercial adsorbent Streamline and the pellicular adsorbent 2% agarose zirconia, in contrast to Figure 5 where there is an apparent partial penetration into the macroporous Celbeads.

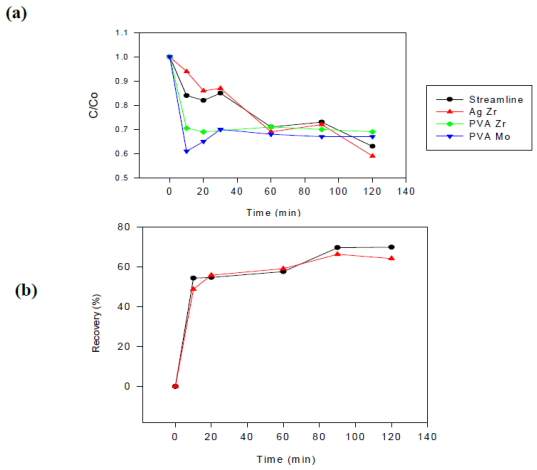

Figure 3. Batch binding and batch elution of HSA nanoparticles. 1004l of adsorbent was challenged with 1.5ml of HSA nanoparticles at a concentration of 2204g/ml in buffer A (10mM Tris-HCl, pH 7.5, 0.02% sodium azide, 0.01% Tween 20) for 2 hours. The decrease in concentration of the feedstock was measured over time (a). The adsorbent was subsequently washed five times with buffer A. The elution was then conducted in 1.5ml of 1.0M NaCl in buffer A and monitored over time. The recovery is expressed as a percentage of the estimated binding (b).

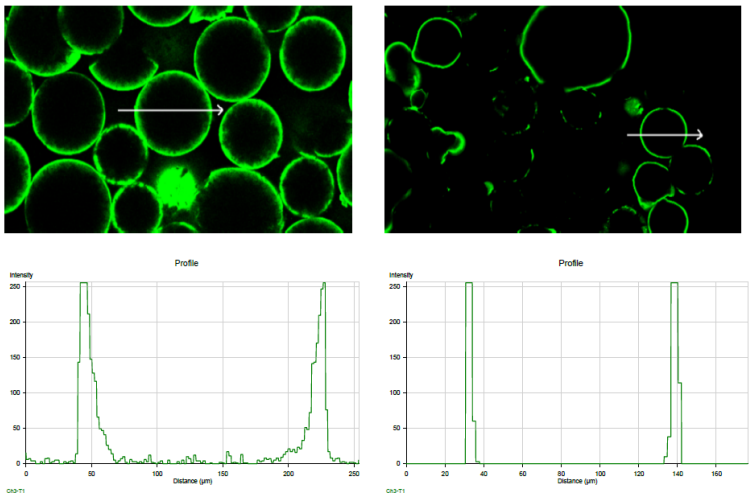

Figure 4. Confocal microscopy images of Streamline (a) and pellicular (b) adsorbents contacted with fluorescently labelled BSA nanoparticles.

4. Conclusions

Adsorbent design implications for the recovery of nanoparticulate products has been investigated with batch binding experiments with fabricated BSA and HSA nanoparticles as surrogate mimics for nanoparticulates such as viruses and plasmid. Customised macroporous and pellicular solid phases were compared to a commercial

microporous adsorbent (Streamline). All of the adsorbent solid phases investigated demonstrated similar binding capacities, with the macroporous adsorbents showing better recoveries (Table 2. and 3.) due to the large pore size which enables easier diffusion of the nanoparticles from the internal structure of the adsorbent solid phase. The customised macroporous and pellicular solid phases showed better bed expansion characteristics than Streamline, which is a process advantage for fluidised bed adsorption of nanoparticulate products. Both pellicular and macroporous solid phases demonstrated good nanoparticle capacities and recoveries with excellent fluidisation properties (Figure 1). There is clearly much scope for the development of custom designed solid phases for fluidised bed recovery of nanoparticulate products.

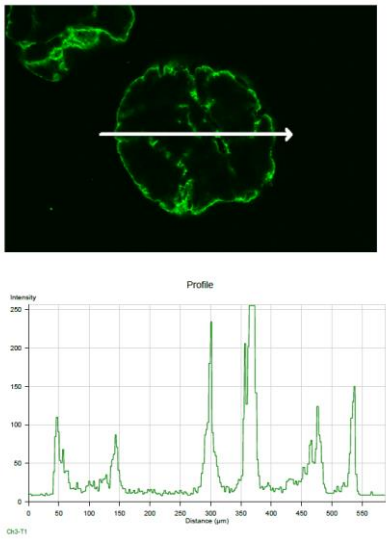

Figure 5. Confocal microscopy images of Celbead adsorbent contacted with fluorescently labelled BSA nanoparticles.

Table 3. Summary of HSA nanoparticle capacities and recoveries from preliminary batch binding experiments.

Adsorbent	Small Ion capacity (mol Cl/ml ads.)	HAS nanoparticle capacity (mg/ml ads.)	HSA nanoparticle capacity (particles/ml ads.)	Recovery %
Streamline	160	2.9574	1.84×10^{13}	~100
2%Agarosezircona	89	2.95	1.99×10^{13}	~100
PVA Mo	27.8	2.66	1.79×10^{13}	
PVA Zr	54.4	2.08	1.4×10^{13}	

Table 3 summarises the adsorptive capacities and recoveries of HSAp calculated from batch adsorption and desorption studies. The capacity was determined by difference analysis of the initial load and the concentration after 120 minutes, whilst the recovery is the protein recovered as percentage of the protein adsorbed.

5. Acknowledgements

The authors gratefully acknowledge Mazandaran University for financial support. Also, many thanks to Mumbai University for supplying a number of adsorbents.

References

1. Peeters OM, de Ranter CJ. 1974. Pathways in thioacetamide hydrolysis in aqueous acid: detection by kinetic analysis. *Journal of the Chemical Society, Perkin Transactions 2* (15): 1832-1835.
2. Rossetti R, Hull R, Gibson JM, Brus LE. 1985. Excited electronic states and optical spectra of ZnS and CdS crystallites in the ≅15 to 50 Å size range: Evolution from molecular to bulk semiconducting properties. *The Journal of Chemical Physics* 82(1): 552-559.
3. Herron N, Wang Y, Eckert H. 1990. Synthesis and characterization of surface-capped, size-quantized cadmium sulfide clusters. Chemical control of cluster size. *Journal of the American Chemical Society* 112(4): 1322-1326.
4. Lewis LN. 1993. Chemical catalysis by colloids and clusters. *Chemical Reviews* 93(8): 2693-2730.
5. Ma J, Huang X, Cheng H, Zhao Z, Qi L. 1996. Preparation of nanosized ZnS particles in water/oil emulsions by microwave heating. *Journal of Materials Science Letters* 15(14): 1247-1248.
6. Motte L, Billoudet F, Lacaze E, Douin J, Pileni MP. 1997. Self-Organization into 2D and 3D Superlattices of Nanosized Particles Differing by Their Size. *The Journal of Physical Chemistry B* 101(2): 138-144.
7. Chen C-C, Herhold AB, Johnson CS, Alivisatos AP. 1997. Size Dependence of Structural Metastability in Semiconductor Nanocrystals. *Science* 276(5311): 398.
8. Asemave K, Abakpa DO, Ligom TT. 1999. Extraction and Antibacterial Studies of Oil from three Mango Kernel obtained from Makurdi - Nigeria. *Progress in Chemical and Biochemical Research* 3(1): 74-80. en.
9. Calandra P, Goffredi M, Liveri VT. 1999. Study of the growth of ZnS nanoparticles in water/AOT/n-heptane microemulsions by UV-absorption spectroscopy. *Colloids and Surfaces A:*

Physicochemical and Engineering Aspects 160(1): 9-13.
10. Dhas NA, Zaban A, Gedanken A. 1999. Surface Synthesis of Zinc Sulfide Nanoparticles on Silica Microspheres: Sonochemical Preparation, Characterization, and Optical Properties. *Chemistry of Materials* 11(3): 806-813.
11. Chai L, Tsamos MK, Tassou AS. 2020. Modelling and Evaluation of the Thermohydraulic Performance of Finned-Tube Supercritical Carbon Dioxide Gas Coolers. *Energies* 13(5).
12. Shamsin Beyranvand H, Mirzaei Ghaleh Ghobadi M, Sarlak H. 2020. Experimental Study of Carbon Dioxide Absorption in Diethyl Ethanolamine (DEEA) in the Presence of Titanium Dioxide (TiO2). *Progress in Chemical and Biochemical Research* 3(1): 55-63. en.
13. Ogbuagu AS-M, Okoye CI. 2020. Physico-chemical characterization of Avocado (Persea americana Mill.) Oil from Tree Indonesian Avocado Cultivars. *Progress in Chemical and Biochemical Research* 3(1): 39-45. en.
14. Basak G, Hazra C, Sen R. 2020. Biofunctionalized nanomaterials for in situ clean-up of hydrocarbon contamination: A quantum jump in global bioremediation research. *Journal of Environmental Management* 256: 109913.
15. Kheirabadi MA, Jafari MH, Alizadeh F, Basiri Z, Oveisi K. 2019. Comparison and Satisfaction of Injured Management System for Students Athlete in the Sport Federations. *Journal of Computational and Theoretical Nanoscience* 16(1): 284-288.
16. Kheirabadi MA, Jafari MH, Alizadeh F, Basiri Z, Oveisi K. 2019. Making an entity-relationship model of the knowledge management process with strategic thinking. *Revista Latinoamericana de Hipertension* 14(1): 55-61.
17. Sara Kashisaz MM. 2018. Implementation of switching law constrained for controlling of switched linear systems. *Amazonia Investiga* 7(15): 367-385.
18. Santharaman P, Venkatesh KA, Vairamani K, Benjamin AR, Sethy NK, Bhargava K, et al. 2017. ARM-microcontroller based portable nitrite electrochemical analyzer using cytochrome c reductase biofunctionalized onto screen printed carbon electrode. *Biosensors and Bioelectronics* 90: 410-417.